CHEMICAL ENGINEERING TRANSACTIONS
VOL. 83, 2021
A publication of AIDIC
The Italian Association of Chemical Engineering
Online at www.cetjournal.it
Guest Editors: Jeng Shiun Lim, Nor Alafiza Yunus, Jiří Jaromír Klemeš

ISBN 978-88-95608-81-5; **ISSN** 2283-9216
DOI: 10.3303/CET2183042

Synthesis of WO_3/g-C_3N_4 Nanocomposite for Photocatalytic CO_2 Reduction Under Visible Light

Beenish Tahir Muhammad Tahir*, Mohd Ghazali Mohd Nawawi

Department of Chemical Engineering, School of Chemical and Energy Engineering, Universiti Teknologi Malaysia (UTM), 81310 Skuda, Johor Bahru, Johor, Malaysia.
mtahir@cheme.utm.my

Greenhouse gas CO_2 emitted through the burning of fossil fuels is a main cause of global warming. Among the different alternatives, photocatalytic conversion of CO_2 using solar energy in the presence of highly efficient photocatalyst is most attractive for the production of solar fuels. In this work, graphitic carbon nitride (g-C_3N_4) dispersed tungsten oxide (WO_3) to construct WO_3/g-C_3N_4 heterojunction was synthesized through hydrothermal approach. The performance of photocatalysts were tested for photocatalytic CO_2 reduction with CH_4 to CO via dry reforming of methane (DRM) under visible light irradiation in a fixed bed photoreactor. The performance of composite catalysts was further tested for photo-catalytic CO_2 reduction via H_2O as reductant and bireforming of methane (BRM) under visible light irradiations. The maximum CO production of 310 µmol g-cat^{-1} h^{-1} was observed over WO_3/g-C_3N_4 composite catalyst which is 2.95 and 8.85 folds higher than using pristine g-C_3N_4 and WO_3 photocatalysts. Using BRM process, production of CO was further increased due to the addition of water into CO_2-methane system. In general, significantly enhanced photocatalytic performance of composite catalyst was obviously due to Z-scheme heterojunction formation with efficient charge carrier separation and good band positions under visible light irradiation. The newly developed composite catalysts can effectively be used for recycling greenhouse gases to fuels using solar energy and would be beneficial for cleaner environment.

1. Introduction

Global warming effects due to CO_2 emitted during fossil fuels combustions and other human activities is a major challenge, the world is facing (Khan and Tahir., 2019). The phototechnology via photocatalytic CO_2 reduction through different reforming technologies has been investigated over the years by many researchers. Besides, methane (CH_4) is another greenhouse gas, emitted from agricultural, fossil fuels and biomass process. The utilizing both CH_4 and CO_2 for the production of synthesis gas (CO and H_2) and higher hydrocarbons is a new development in the reforming technologies. The most commonly employed approach for the utilization of both CO_2 and CH_4 includes CO_2 reforming with CH_4 called dry reforming of methane (DRM) (Moral et al., 2018), which has several benefits such as minimizing their level in the atmosphere, and producing equimolar syngas mixture (H_2/CO=1.0)

In thermal reforming, DRM operates under higher reaction temperature, which produces coke and provides instability to catalyst. Using phototechnology, higher activity and photostability can be obtained, in addition of low-cost process for chemicals and fuels production. During the last few years, there has been growing research on photocatalytic CO_2 reduction through DRM under UV and visible light irradiations. Different photocatalysts such as La-doped TiO_2 (Tahir et al., 2017), Pt-loaded TiO_2 (Han et al., 2015), and Au/Rh modified TNTs (László et al., 2016) have been investigated for photocatalytic DRM process under UV-light irradiations.

Recently, graphitic carbon nitride (g-C_3N_4), a 2D layered semiconductor material, is under investigation due to several benefits such as cheaper, easy to prepare and high stability (thermal/chemical). In addition, g-C_3N_4 is active under visible light irradiations due to narrow bang gap energy (E_g~ 2.70 eV) (Shi et al., 2020), compared to wide band gap energy semiconductors such as TiO_2 (E_g~ 3.20 eV). Recently, there has been growing interest on the use of g-C_3N_4 photocatalyst for photocatalytic CO_2 reduction through different CO_2

Paper Received: 07/07/2020; Revised: 05/10/2020; Accepted: 17/10/2020
Please cite this article as: Beenish T., Muhammad T., Mohd Nawawi M.G., 2021, Synthesis of WO_3/g-C_3N_4 Nanocomposite for Photocatalytic CO_2 Reduction Under Visible Light, Chemical Engineering Transactions, 83, 247-252 DOI:10.3303/CET2183042

reduction process. In this perspective, the use of Cu/g-C_3N_4 (Tahir et al., 2017) for DRM under visible light irradiation was investigated. In addition of metals lading, coupling g-C_3N_4 with other semiconductors can be a promising approach to maximize charges separation with higher visible light absorption. Tungsten oxide (WO_3) is a very promising cocatalyst due to its lower band gap energy and higher oxidation potentials (Bafaqeer et al., 2019). In this perspective WO_3/g-C_3N_4 for enhanced photo-catalytic H_2 production has been reported (Fu et al., 2019). The conversion of greenhouse gases over WO_3/g-C_3N_4 catalyst for the production of synthesis gas and valuable fuels would be beneficial for efficient photo-catalytic CO_2 reduction under visible light.

In this study, fabrication of WO_3/g-C_3N_4 heterojunction composite for photocatalytic CO_2 reduction via dry reforming of methane (DRM) and bireforming of methane (BRM) under visible light has been investigated. The photocatalysts were synthesized using hydrothermal approach. The photoactivity of WO_3/g-C_3N_4 was further examined in different reforming systems to understand the role of sacrificial reagents in CO_2 reduction process. The effect of irradiation time and reaction mechanism to understand the role of each component in the composite catalyst was further investigated.

2. Experimental

2.1 Materials synthesis and characterization

The bulk g-C_3N_4 was prepared by heating melamine (Sigma Aldrich) at 550 ºC for 2 h in a muffle furnace under air atmosphere. The product obtained was grinded to get bulk g-C_3N_4, which was further treated with acetic acid and dried overnight to get g-C_3N_4 (Tahir et al., 2020). For the synthesis of WO_3/g-C_3N_4 composite, ultrasonic assisted physical mixing approach was employed. Typically, 1 g of g-C_3N_4 was dispersed in a methanol and stirred for 6 12 h to get uniform dispersion. Afterwards, specific amount of WO_3 (50 wt% g-C_3N_4) dispersed in a methanol was added to above solution under stirring for another 12 h. Finally, samples were dried at 100 ˚C overnight to get WO_3/g-C_3N_4 composite samples. All the samples were characterized using XRD, PL< SEM, TEM and UV visible techniques. X-ray diffraction (XRD, RIGAKU), operated with Cu-Kα radiation at λ=0.154178 nm, 40 kV and 30 mA. The morphologies were obtained by FESEM, ZEISS Crossbeam 340 and TEM, HITACHI HT7700. The PL analysis was conducted using Lab RAM HR Evolution, HORIBA and UV-visible analysis was conducted using Cary 100 Agilent, Model G9821 A.

2.2 Photoactivity test

The photoactivity test was conducted in a stainless steel photoreactor with diameter 6 cm, lighting surface 28 cm^2 and total volume 150 cm^3. The reactor was equipped was a glass window for passing the light irradiations. The experiments were conducted for photocatalytic CO_2 reduction using H_2O, H_2, and CH_4 reducing agents. A HID Xenon lamp with power 35 W with wavelength 420 nm and intensity 20 mW cm^{-2} was used as a source of visible light. The lamp was located at the top of glass reactor and equipped with cooling fans to remove heat. Specifically, 150 mg powder photocatalyst was evenly dispersed at the bottom of stainless-steel chamber. High purity gases (CO_2, 99.99 % and CH_4, 99.99 %), regulated by mass flow controllers (MFC), were passed through the reactor to remove the air and to saturate the catalyst surface. The CO_2/CH_4 feed ratio of 1.0 was used in all the experiments. All the experiments were conducted under normal temperature and atmospheric pressure. The products were analysed using gas chromatograph (GC 6890 N). The Carboxen-1010 PLOT Capillary Column equipped with a thermal conductivity detector (TCD) and a flame ionized detector (FID) was used for the separation of CO, CH_4, CO and H_2 products.

3. Results and discussion

3.1 Catalyst characterization

Figure 1a shows XRD analysis of g-C_3N_4 and WO_3/g-C_3N_4 composites. Obviously, g-C_3N_4 presents two peaks positioned at 2-thetea of 13.10˚ and 27.44˚, relating to polymeric structure graphitic carbon nitride. Similarly, WO_3 peaks in WO_3/g-C_3N_4 composite were appeared at 2-θ of 23.01º, 23.52º, 24.25º, 26.49˚ 28.55º, 28.83º, 33.17º, 33.47˚, 34.07º, 35.52º, 41.39º,41.83º,47.15º, 48.21º, and 49.81º, confirming the presence of WO_3 in the composite sample (Card no 01-083-0950) (Tahir et al., 2020). More importantly, all the peaks relating to g-C_3N_4 were appeared in the composite of WO_3/g-C_3N_4, confirming, successful fabrication of composite through ultrasonic approach. Figure 1b presents photoluminescence (PL) plots of pristine g-C_3N_4 and WO_3/g-C_3N_4 composite. Obviously, highest PL intensity was obtained in pristine g-C_3N_4 due to fast charges recombination rate. However, a gradual declined in PL intensity was observed when g-C_3N_4 was coupled with WO_3. This declined in PL intensity was due to faster charge carrier separation with hindered recombination rate over the WO_3/g-C_3N_4 composite sample. This further confirms successful fabrication of WO_3/g-C_3N_4 heterojunction.

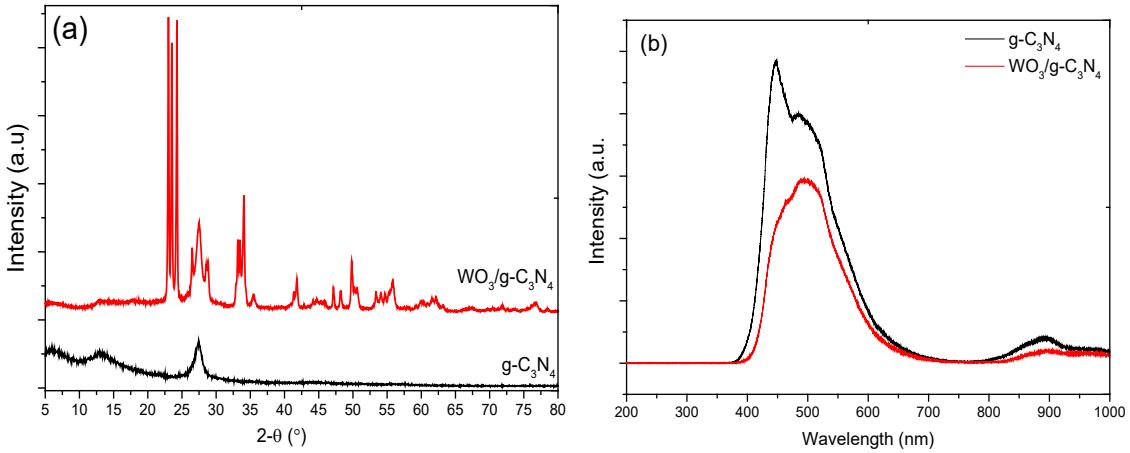

Figure 1: (a) X-ray diffraction patterns of g-C_3N_4 and WO_3/g-C_3N_4 composite samples; (b) Photoluminescence analysis for g-C_3N_4 and WO_3/g-C_3N_4 samples

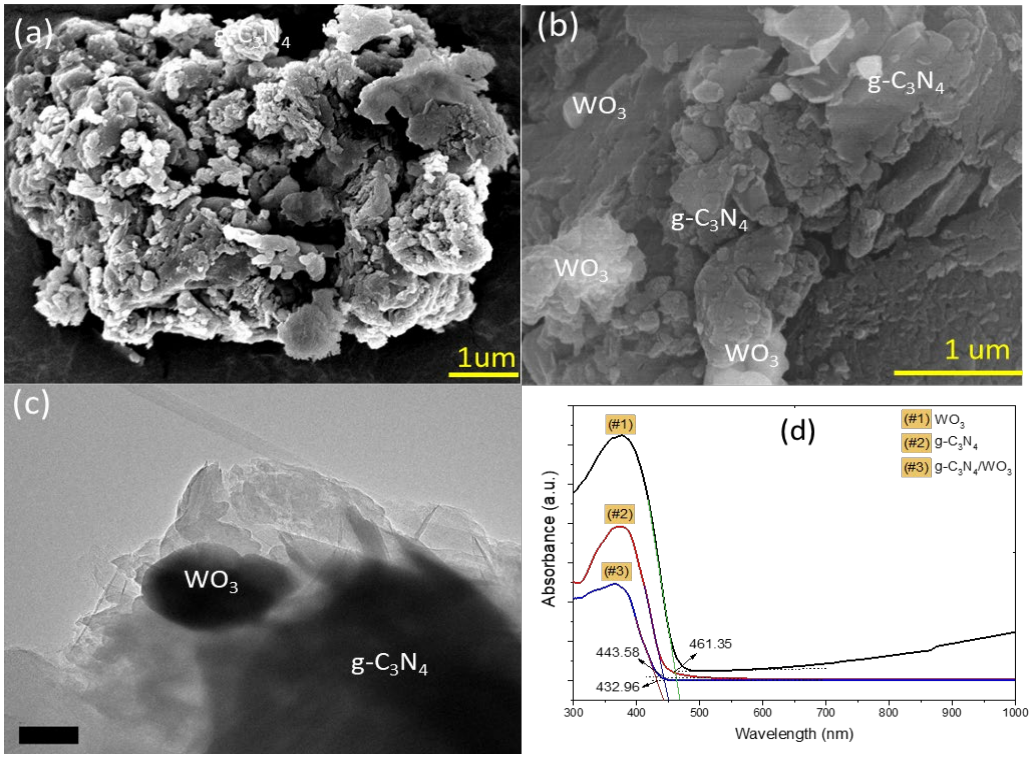

Figure 2: FE-SEM analysis of (a) g-C_3N_4 and (b) WO_3/g-C_3N_4 samples; (c) TEM analsyis of WO_3/g-C_3N_4 samples, (d) UV-visible analysis of g-C_3N_4, WO_3 and WO_3/g-C_3N_4 photocatalysts.

The morphology of g-C_3N_4 and WO_3/g-C_3N_4 composite were further investigated using FESEM and TEM characterization techniques and results are demonstrated in Figure 2. Figure 2a show morphology of g-C_3N_4, in which, obvious two-dimensional folded sheets of graphitic carbon nitrides could be observed. FESEM image in Figure 2b shows morphology of WO_3/g-C_3N_4 composite. It could be seen a good dispersion of WO_3 with g-C_3N_4 nanosheets. A further interaction of WO_3 with 2D g-C_3N_4 nanosheets could be observed in TEM image as demonstrated in Figure 2c. Obviously, WO_3 microspheres were distributed over g-C_3N_4 nanosheets, producing a heterojunction between both the semiconductors.

The UV-visible analysis was further conducted to determine band gap energy and light absorption trends of g-C_3N_4 and WO_3/g-C_3N_4 samples. Obviously, both g-C_3N_4 and WO_3/g-C_3N_4 has response of light absorption under visible light. The light absorption wavelengths of 461.35, 443.58 and 432.96 nm were obtained for WO_3,

g-C_3N_4 and WO_3/g-C_3N_4 samples. This confirms higher visible light absorption of the samples and would be beneficial for photocatalytic CO_2 reduction applications (Tahir et al., 2020). The band gap energies of 2.70, 2.81 and 2.88 eV were obtained for WO_3, g-C_3N_4 and WO_3/g-C_3N_4 samples.

3.2 Photocatalytic CO_2 reduction

The photoactivity test of g-C_3N_4, WO_3 and WO_3/g-C_3N_4 for photocatalytic CO_2 reduction with CH_4 in the presence of water through bi-reforming of methane (BRM) under visible light irradiations in a fixed bed photoreactor. The amount of photocatalyst loaded was 0.15 g, dispersed uniformly inside the reactor. The feed ratio of CO_2/CH_4 of 1.0 was employed for all the experiments. All the reactions were conducted at normal temperature and atmospheric pressure.

Figure 3a shows photocatalytic CO_2 reduction for the production CO evolution over g-C_3N_4, WO_3 and WO_3/g-C_3N_4 photocatalysts during photocatalytic CO_2 reduction with H_2O/CH_4 photocatalysts. Using pure WO_3, 35 µmol g-cat^{-1}h^{-1} for CO was detected. Comparatively, 105 µmol g-cat^{-1}h^{-1} of CO was obtained over g-C_3N_4 photocatalyst. Obviously, lower photoactivity was attained over WO_3 due to its reduction potential (+0.76 eV) (Ye and Web, 2019), which is more positive than is required for CO_2 reduction (-0.48 eV). Besides, g-C_3N_4 has 2D layered structure, and efficient charges separation efficiency for photocatalytic reaction in addition of higher reduction potential (CB -1.20 eV). When, WO_3/g-C_3N_4 were coupled highest photoactivity of 310 µmol g-cat^{-1}h^{-1} of CO was attained. This significantly enhanced photoactivity of WO_3/g-C_3N_4 composite was evidently due to faster charges separation with good oxidation and reduction potentials for DRM reaction under visible light irradiations (Guo et al., 2020). This confirms significantly enhanced performance of WO_3/g-C_3N_4 composite and it can be further employed for investigating different reforming reactions.

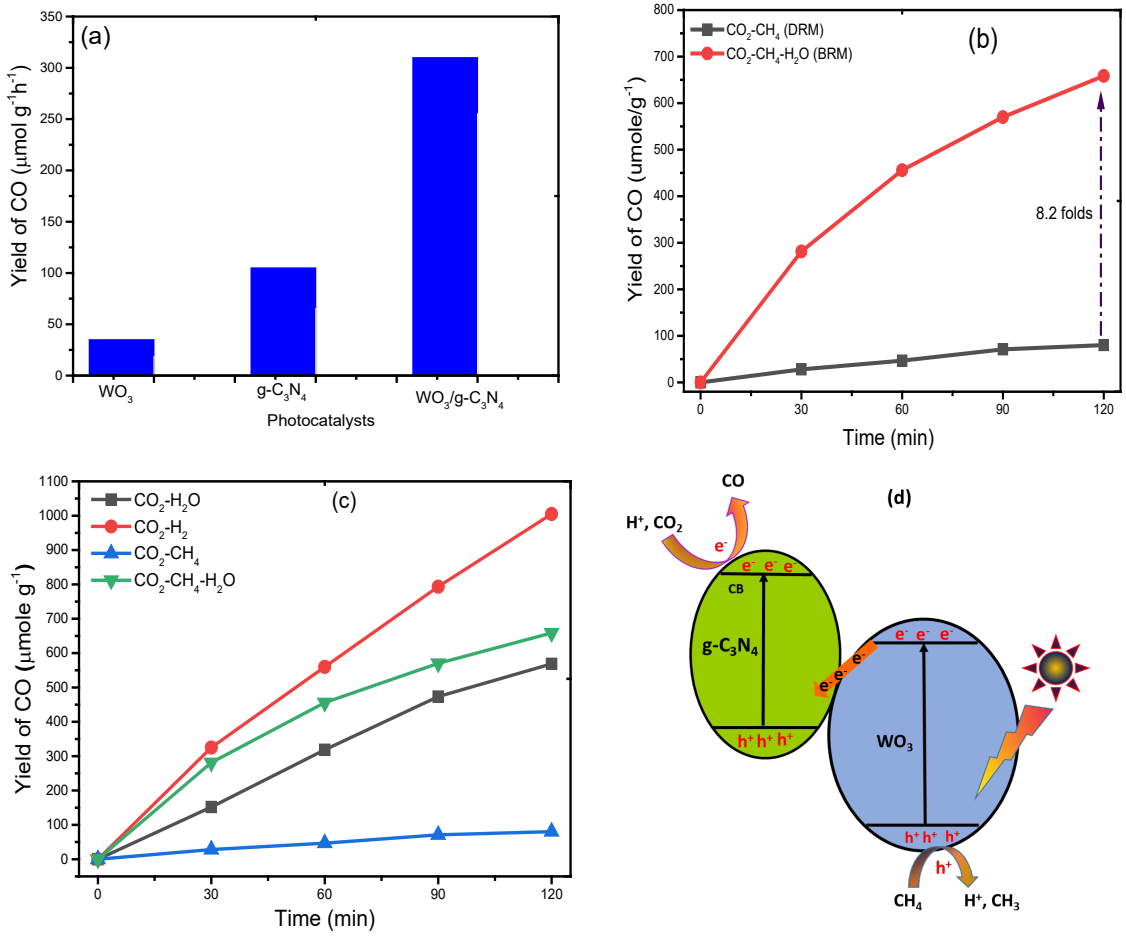

Figure 3: (a) Photocatalytic CO_2 reduction by CH_4/H_2O to CO over different catalysts; (b) Photocatalytic DRM and BRM for CO_2 reduction over WO_3/g-C_3N_4; (c) Performance analysis of reforming systems for CO_2 reduction to CO; (d) proposed schematic mechanism of CO_2 reduction to CO over WO_3/g-C_3N_4 composite.

The performance of WO_3/g-C_3N_4 composite catalyst was further tested in different reforming reactions such as DRM, BRM and RWGS reaction. The production of CO in Figure 3b shows 8.2 folds-higher production of CO using BRM process compared to DRM process under the same reaction conditions. The higher photocatalytic activity for CO evolution through BRM process was due to adding water (H_2O) in CO_2/CH_4 feed system. The water provides higher number of protons (H^+) with the involvement of lower light energy. This confirms BRM process is more efficient for maximizing the photoactivity of WO_3/g-C_3N_4 composite due to the presence of both methane/waters reducing agents with CO_2 during photocatalysis process.

The performance of WO_3/g-C_3N_4 composite catalyst was further tested in different photocatalytic systems such as reduction of CO_2 with H_2O, photocatalytic reversed water gas shift reaction (RWGSR), DRM and BRM reactions as shown in Figure 3c. It could be seen that highest CO evolution rate was attained during CO_2 reduction in the presence of hydrogen through RWGS reaction. Using DRM process lowest CO production was obtained due to high stability of CO_2 and CH_4 molecules. Using water and CO_2, higher amount of CO was evolved compared to DRM reaction, but lower than RWGS and BRM reactions. All these findings confirm that not only photocatalyst, but reforming reactions are also important to maximize photocatalysis process. The selection of both photocatalyst and reducing agents are crucial for selective production of fuels during CO_2 conversion under visible light irradiation. Previously, photocatalytic CO_2 reduction with H_2O over Pd–Au/TiO_2–WO_3 for CO and CH_4 production (Zhu et al., 2018), higher CO/CH_4 production over WO_3-TiO_2/Cu_2ZnSnS_4 (Raza et al., 2020) and WO_3/g-C_3N_4 with CO and CH_4 production (Li et al., 2020) have been investigated. Comparatively, efficient photocatalytic CO_2 reduction with CO and H_2 production through DRM and BRM was observed over WO_3/g-C_3N_4 composite through the involvement of Eq(1) and Eq(2).

$$\mathrm{CH_4 + CO_2 \longrightarrow 2CO + 2}H_2 \quad \Delta\,\mathrm{H_{298K}} = +247\mathrm{kJ/mol} \tag{1}$$

$$\mathrm{3CH_4 + CO_2 + 2H_2O \longrightarrow 4CO + 8H_2} \quad \Delta\,\mathrm{H_{298K}} = +220\mathrm{kJ/mol} \tag{2}$$

3.3 Reaction mechanism

The photocatalytic CO_2 reduction using water/methane reducing agnets over WO_3/g-C_3N_4 composite under visible light involves oxidation and reduction reaction through the involvement of electrons and holes has been illustarted in Figure 3d. When visible light strike over the composite catalyst WO_3 is activated first due to its lower bandgap energy (E_g~ 2.70) as illustarted in Eq(3), produicng electrons and holes. As the CB of WO_3 is more positive (CB~ 0.74) (Ye and Wen., 2019) than g-C_3N_4 conduction band (CB~ -1.20). The photogenerated electrons have potential to transfer from CB of WO_3 towards VB of g-C_3N_4, enabling their efficient separation (Eq4). The photogenerated electrons are consued during CO_2 reduction process with CO production and holes were consumed for water and methane oxidation through the reactions in Eqs(5) to (7).

$$WO_3 \xrightarrow{h\nu} WO_3(e^-) + WO_3\,(h^+) \tag{3}$$

$$g - C_3N_4 + WO_3(e^-) \longrightarrow g - C_3N_4(e^-) + WO_3 \tag{4}$$

$$\mathrm{CO_2} + 2H^+ + 2e^- \longrightarrow \mathrm{CO{+}2H_2}O \tag{5}$$

$$H_2\mathrm{O{+}2h^+} \xrightarrow{h\nu} \mathrm{2H^+{+}1/2O_2} \tag{6}$$

$$\mathrm{CH_4{+}h^+} \xrightarrow{h\nu} H^+ + \bullet\,\mathrm{CH_3} \tag{7}$$

Accoridng to experimental results, CO_2 was efficiently converted to CO through different reforming reactions such as DRM, BRM and RWGS reactions. The significantly enhanced phototacivity for CO_2 reduction over WO_3/g-C_3N_4 composite was due to Z-scheme heterojunction formation with efficient charges separation.

4. Conclusions

The WO_3/g-C_3N_4 composite catalyst was successfully synthesized and tested for photocatalytic CO_2 reduction under visible light irradiations. In Z-scheme WO_3/g-C_3N_4 composite, efficient charge separation was observed enabling more production of CO during photocatalytic dry and bireforming reactions. The highest CO production of 310 μmol g-cat^{-1}h^{-1} over WO_3/g-C_3N_4 composite was achieved. The performance of different reforming reactions such as dry reforming of methane, bireforming of methane and reverse water gas shift

reactions were further investigated. Using BRM and RWGS reactions, highest amount of CO was evolved under the same reaction conditions. It could be concluded that WO_3/g-C_3N_4 heterojunction is a promising photocatalyst for photocatalytic CO_2 reduction under visible light irradiation and can be employed in other solar energy assisted applications. due to efficient charges separation and higher visible light absorption.

Acknowledgements

This work is sponsored by Ministry of Education (MOE), Malaysia under Long Term Research Grant Scheme (LRGS NanoMITE, 203/PJKIMIA/6720009 and UTM, Vot R. J130000.7851.4L900).

Reference

Bafaqeer A., Tahir M., Amin N.A.S., 2019, Well-designed ZnV_2O_6/g-C_3N_4 2D/2D nanosheets heterojunction with faster charges separation via pCN as mediator towards enhanced photocatalytic reduction of CO_2 to fuels, Applied Catalysis B: Environmental, 242, 312-326.

Fu J., Xu Q., Low J., Jiang C., Yu J., 2019, Ultrathin 2D/2D WO_3/g-C_3N_4 step-scheme H_2-production photocatalyst, Applied Catalysis B: Environmental, 243, 556-565.

Guo R.-t., Liu X.-y., Qin H., Wang Z.-y., Shi X., Pan W.-g., Fu Z.-g., Tang J.-y., Jia P.-y., Mia Y.-f., Gu J.-w, 2020, Photocatalytic reduction of CO_2 into CO over nanostructure Bi_2S_3 quantum dots/g-C_3N_4 composites with Z-scheme mechanism, Applied Surface Science, 500, 1-9.

Han B., Wei W., Chang L., Cheng P., Hu Y. H., 2015, Efficient Visible Light Photocatalytic CO_2 Reforming of CH_4, ACS Catalysis, 6 (2), 494-497.

Khan A. A., Tahir M., 2019, Recent advancements in engineering approach towards design of photo-reactors for selective photocatalytic CO_2 reduction to renewable fuels, Journal of CO_2 Utilization, 29, 205-239.

László B., Baán K., Varga E., Oszkó A., Erdőhelyi A., Kónya Z., Kiss J., 2016, Photo-induced reactions in the CO_2-methane system on titanate nanotubes modified with Au and Rh nanoparticles, Applied Catalysis B: Environmental, 199, 473-484.

Li X., Song X.C., Cheng Ma. Y., Shen D., Zhang S., Liu W., Huo P., Wang H., 2020, Direct Z-Scheme WO3/Graphitic Carbon Nitride Nanocomposites for the Photoreduction of CO_2, ACS Applied Nano Materials, 3 (2), 1298-1306.

Moral A., Reyero I., Alfaro C., Bimbela F., Gandia L.M., 2018, Syngas production by means of biogas catalytic partial oxidation and dry reforming using Rh-based catalysts, Catalysis Today, 299, 280-288.

Raza A., Shen H., Haidry A.A., Sun L., Liu R., Cui S., 2020, Studies of Z-scheme WO_3-TiO_2/Cu_2ZnSnS_4 ternary nanocomposite with enhanced CO_2 photoreduction under visible light irradiation, Journal of CO_2 Utilization, 37, 260-271.

Shi H., Du J., Hou J., Song W.C., Li K., Gurzadyan G.G., Guo X., 2020, Solar-driven CO_2 conversion over Co^{2+} doped 0D/2D TiO_2/g-C_3N_4 heterostructure: Insights into the role of Co^{2+} and cocatalyst, Journal of CO_2 Utilization, 38, 16-23.

Tahir B., Tahir M., Amin N.A.S., 2017, Photocatalytic Carbon Dioxide and Methane Reduction to Fuels over La-Promoted Titanium Dioxide Nanocatalyst, Chemical Engineering Transactions, 56, 1123-1128.

Tahir, B., Tahir M., Amin N.A.S., 2017, Photocatalytic Carbon Dioxide Reduction to Fuels Over CuLoaded g-C_3N_4 Nanocatalyst under Visible Light, Chemical Engineering Transactions, 56, 403-408.

Tahir B., Tahir M., Nawawi M.G.M., 2020, Highly stable 3D/2D WO_3/g-C_3N_4 Z-scheme heterojunction for stimulating photocatalytic CO_2 reduction by H_2O/H_2 to CO and CH_4 under visible light, Journal of CO_2 Utilization, 41, 101270.

Ye L., Wen Z., 2019, $ZnIn_2S_4$ nanosheets decorating WO_3 nanorods core-shell hybrids for boosting visible-light photocatalysis hydrogen generation, International Journal of Hydrogen Energy, 44 (7), 3751-3759.

Zhu Z., Huang W.-R., Chen C.-Y., Wu R.-J., 2018, Preparation of Pd–Au/TiO_2–WO_3 to enhance photoreduction of CO_2 to CH_4 and CO, Journal of CO_2 Utilization, 28, 247-254.